

POLITECNICO DI MILANO



ORBITAL MECHANICS FINAL ASSIGNMENT  
INTERPLANETARY TRAJECTORIES & ORBITAL PERTURBATIONS

---

Group 10

Teodoro Bonariol (941028)  
*teodoro.bonariol@mail.polimi.it*

Alexia Cantoni (945126)  
*alexia.cantoni@mail.polimi.it*

Anita Capelli (939522)  
*anita.capelli@mail.polimi.it*

Adrian Burton Parisi (940789)  
*adrianburton.parisi@mail.polimi.it*

February 1, 2020

# 1 Interplanetary Explorer Mission Analysis

The PoliMi Space Agency has provided a challenge with the main goal is to analyse and design an interplanetary trajectory between two planets, Jupiter to Venus, using a third planet, Earth, to perform a Powered Gravity Assist (PGA) manoeuvre. The trajectory of the overall mission is dependent on two main factors: the propellant cost and the time of flight to complete the mission. Therefore, the design analysis is a minimisation problem and the minimisation of the propellant cost was deemed of more importance and will be denoted as the mission cost in regards to this report.

By performing a PGA manoeuvre at the intermediary planet, the total mission cost could potentially be reduced on the account of the planet providing the majority of velocity vector change required for an efficient trajectory to the destination planet.

## 1.1 Mission constraints

The main constraint is linked with the time window of the mission: the departure and arrival dates must lie within 01/01/2020 - 01/01/2060. Furthermore, during the PGA manoeuvre analysis, it is necessary to check if the spacecraft does not crash onto the intermediate planet's surface or enter its denser layers of the atmosphere. As Earth is the intermediate planet at which the PGA occurs the minimum orbital radius,  $r_{min}$ , allowed during the manoeuvre will be,

$$r_{min} = R_E + z$$

where  $R_E = 6378\text{km}$ , the radius of Earth, and  $z = 150\text{km}$ , an altitude corresponding to low Earth orbit.

## 1.2 Model Approximations

Several approximations have been made in order to simplify and reduce the calculations required for computing the trajectories. The patched conic approximation reduces an  $n$ -body problem to a 2-body problem. This method is based on the concept of sphere of influence around planetary bodies and, whilst the spacecraft is outside the sphere of influence of a planet, the gravitational effect of the planet on the spacecraft is neglected. Therefore, during the interplanetary trajectories the spacecraft will solely be affected by the gravitational attraction of the Sun.

The PGA manoeuvre has been considered as instantaneous one on account of the time taken for the manoeuvre is negligible with respect to the time required to accomplish the entire mission. This approximation is justified in Section 1.5.2. In addition, during this manoeuvre the orbiting bodies around the Earth, such as satellites or space debris, have not been included.

There are several perturbations which can potentially affect the orbital trajectory of the spacecraft such as solar radiation pressure during the interplanetary legs, gravitational perturbations from the other planets, and atmospheric drag during the PGA manoeuvre around Earth. However, these have all been neglected to greatly simplify the model and reduce computational requirements. Moreover, due to the minimal affects of non-spherical gravitational perturbations at large distances, all planets have been assumed to have a perfect spherical distributions of mass.

### 1.2.1 Moon Sphere of Influence

As the PGA manoeuvre is conducted around Earth, it should be reasonable to assume that the presence of Moon will affect the path of the spacecraft, as a consequence the problem becomes a 3 body problem which leads to solving a more complex set of equations.

The Moon involvement is purely linked to the fact that it has a non negligible mass with respect to the Earth, therefore its sphere of influence is comparable with the Earth one, so we should also take in account the presence of the Moon in the computation of the PGA manoeuvre. Furthermore, its distance from Earth is within the Earth's sphere of influence thus, the position of the Moon should be considered to avoid a

collision or affect the path of the spacecraft. However, in order to reduce the complexity of the problem, the presence of the Moon has been neglected.

### 1.2.2 Synodic Period

The evaluation of the synodic period,  $T_{synodic}$ , for two planet system is given by,

$$T_{synodic} = \frac{T_1 T_2}{T_2 - T_1} \quad (1)$$

where  $T_1$  and  $T_2$  are the period of Planet 1 and Planet 2, respectively.[1]

The calculation of the synodic period of a three planet system required a different methodology. An algorithm was developed to calculate the positions of the planets relative to each other and store the dates at which the planets relative true anomaly were within  $1^\circ$  of each other. The results of this algorithm for the current millennia are shown in Table 1.

Day	Month	Year
25	9	2031
18	1	2142
23	10	2186
16	2	2297
9	6	2407
5	7	2562
2	8	2717
16	3	2938
18	12	2982

Table 1: Dates in which Venus, Earth, and Jupiter align over the current millennium within a tolerance of  $1^\circ$  of each other.

As the re-alignment of the three planets does not occur on multiple occasions within even the current century, the justification of reducing the departure time window to reduce the required calculations cannot be made. Therefore, the entire time window must be considered during the calculations for the optimal interplanetary trajectory.

## 1.3 Interplanetary Trajectory Calculation

The LambertMR algorithm, a solver for the Lambert problem provided by the COMPASS research team at the Politecnico di Milano, was utilised to design the interplanetary trajectories from Jupiter to Earth, where the PGA manoeuvre occurs, and then from Earth to Venus. The position parameters required for the LambertMR were generated by calculating the orbital elements of the corresponding planets by taking advantage of the function *uplanet*, an ephemeris algorithm also provided by the COMPASS team, and converting to a Heliocentric Cartesian reference system. Additionally, the LambertMR requires the time of flight of the interplanetary trajectory as an input. This will be given by the optimisation algorithm and discussed in Section 1.4.

The initial and final velocities output by the LambertMR function, corresponding to the initial and final positions, and the time of flight provided, are exploited to achieve the total  $\Delta V$  for a given transfer. All calculations within LambertMR correspond to zero-rotation counter-clockwise Lambert transfers.

### 1.3.1 Powered Gravity Assist Manoeuvre

As aforementioned, the patched conic method is employed to simplify the model during interplanetary trajectories. However, once the spacecraft is within the sphere of influence of a planet more detailed calculations

are necessary. The velocity inputs for the PGA manoeuvre were attained from the outputs of the LambertMR algorithm from both interplanetary trajectories.  $\vec{v}_\infty^-$ , the velocity vector upon entering the sphere of influence of Earth equates the final heliocentric velocity vector of the interplanetary trajectory between Jupiter and Earth, whereas  $\vec{v}_\infty^+$  is the velocity vector at the time of leaving the sphere of influence of Earth that equates the initial velocity required for the interplanetary trajectory between Earth and Venus. Both  $\vec{v}_\infty^-$  and  $\vec{v}_\infty^+$  are in the reference frame of the corresponding planet.

As the mission requires travelling from an outer planet to an inner planet during the PGA manoeuvre the velocity of the spacecraft needs to decrease. Therefore, the spacecraft will perform effectively a leading flyby manoeuvre as shown in Figure 1.

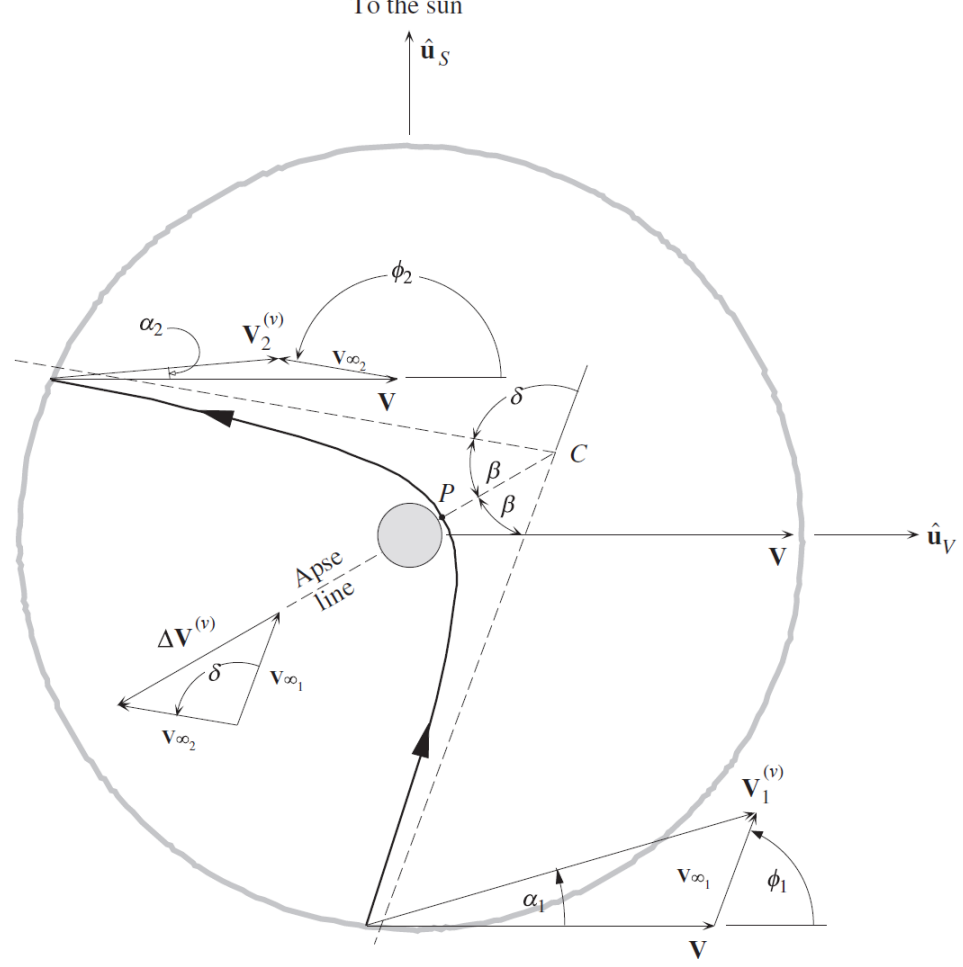


Figure 1: A leading flyby manoeuvre used to reduce the velocity of a spacecraft with the subscript 1 and 2 corresponding to - and +, respectively.[2]

In a simple, ballistic flyby  $\vec{v}_\infty^- = \vec{v}_\infty^+$ , but in order to obtain the necessary velocities required for the second interplanetary trajectory a burn manoeuvre at the perigee is required, thus this produces two asymmetric hyperbolic branches and adding to the current mission cost, where  $\vec{v}_\infty^- \neq \vec{v}_\infty^+$ . The angle between the two velocity vectors is known as the turning angle,  $\delta$ , and is defined as

$$\delta = \delta(\vec{v}_\infty^-, \vec{v}_\infty^+) = \cos^{-1} \left( \frac{\vec{v}_\infty^- \cdot \vec{v}_\infty^+}{|\vec{v}_\infty^+| |\vec{v}_\infty^-|} \right) \quad (2)$$

The turning angle however, can also be made up of the angles of each of the hyperbolic arms denoted by  $\delta^-$  and  $\delta^+$  for the incoming and outgoing hyperbolic arms, respectively. The inclusion of the individual turning angles is advantageous in the calculation of the radius of perigee, the only unknown of the PGA manoeuvre. The equation for the turning angle for a given perigee radius and  $\vec{v}_\infty^\pm$  is defined by

$$\delta^\pm = \delta^\pm(r_p, \vec{v}_\infty^\pm) = 2 \sin^{-1} \left( \left[ 1 + \frac{r_p |\vec{v}_\infty^\pm|^2}{\mu} \right]^{-1} \right) \quad (3)$$

The total turning angle of the PGA manoeuvre can then be found by the combination of the individual turning angles of each hyperbolic arm with,

$$\delta = \frac{\delta^-}{2} + \frac{\delta^+}{2} \quad (4)$$

Therefore, in order to determine the perigee radius root-finding method, the fsolve algorithm provided by the Matlab platform, was employed to solve the following implicit equation

$$\delta - \left( \frac{\delta^-}{2} + \frac{\delta^+}{2} \right) = 0 \quad (5)$$

The radius of Earth was imposed as the initial solution to the root finding method and if the method converged, the perigee radius was checked in order to not intersect the Earth or Earth's atmosphere as aforementioned in Section 1.1.

## 1.4 Optimisation Algorithm

The optimisation algorithm created is a combination of a Monte Carlo method coupled with gradient based optimisation. The ideology behind this approach is to efficiently and explore the complete dimensional space of the three possible dates for departure, PGA manoeuvre, and arrival without the inclusion and complexity of an adaptive grid based approach.

---

**Algorithm 1:** High level optimisation algorithm employed to find the global minima.

---

**Input :** Earliest departure date, latest arrival date, and No. of converges to complete

**Output:**  $\Delta V_{min}$ ,

Generate array of all possible dates

**while** not reached set number of converged optimisations **do**

// Corresponding to the departure, fly by, and arrival dates

Randomly choose 3 different dates within the date array

**if** departure date < flyby date < arrival date **then**

**while** not converged **do**

Generate 3D stencil from the current dates

Calculate minimum  $\Delta V_{current}$ , ToF, and check if crashed and converged

**if** not crashed and ( $\Delta V_{current} < \Delta V_{min}$ ) **then**

Set  $\Delta V_{min} = \Delta V_{current}$

---

The Monte Carlo method contribution to the optimiser is solely to randomly generate the initial dates to pass into the gradient based optimiser. This is in place of a typical grid based search where the dates will be iterated sequentially. The gradient based optimisation however, is the standard hill stepping algorithm extended to 3D by treating the departure, PGA manoeuvre, and arrival dates as individual dimensions with a fitness function of minimising  $\Delta V$ . A high level description of the algorithm is shown in Algorithm 1.

## 1.5 Results

The optimiser was run to achieve 5000 successful converges without the spacecraft colliding with Earth during the PGA manoeuvre and conducted within Matlab 2019b. The optimum dates found during this run are shown in Table 2 with the corresponding snapshots of the solar system at the departure, PGA manoeuvre, and arrival dates shown in Figures 2, 3, and 4, respectively.

	Departure	Arrival	$\Delta V$	ToF
Jupiter → Earth	11/11/2034	13/05/2037	6.2817 km/s	914 days
Earth → Venus	13/05/2037	12/09/2038	7.0172 km/s	487 days

Table 2: The departure and arrival dates for the interplanetary trajectories.  $\Delta V$  requirements and the time of flight for the

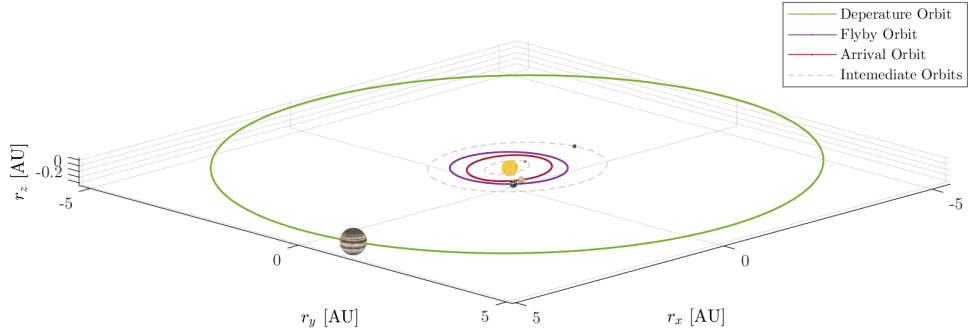


Figure 2: The relative positions of the planets at the date of the departure from Jupiter.

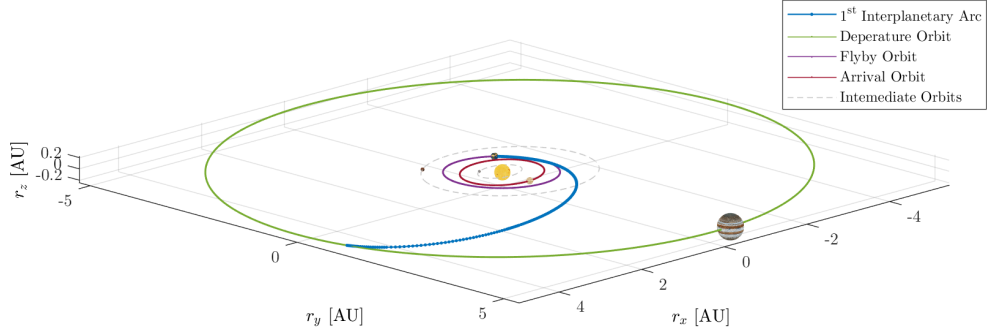


Figure 3: The relative positions of the planets at the date of the PGA manoeuvre with the inclusion of the path taken of the spacecraft whilst travelling from Jupiter to Earth.

### 1.5.1 Powered Gravity Assist Manoeuvre

The  $\Delta V$  for the PGA manoeuvre is relatively low in comparison to the  $\Delta V$  for departure and arrival of the planets. This is further evident in the difference between semi-major axis and eccentricity for the incoming and outgoing hyperbolic arms in Table 4. Moreover, the constraint of  $r_{min}$  discussed in Section 1.1 is fully respected, as the altitude of perigee being 643.0 km, as shown in Table 3.

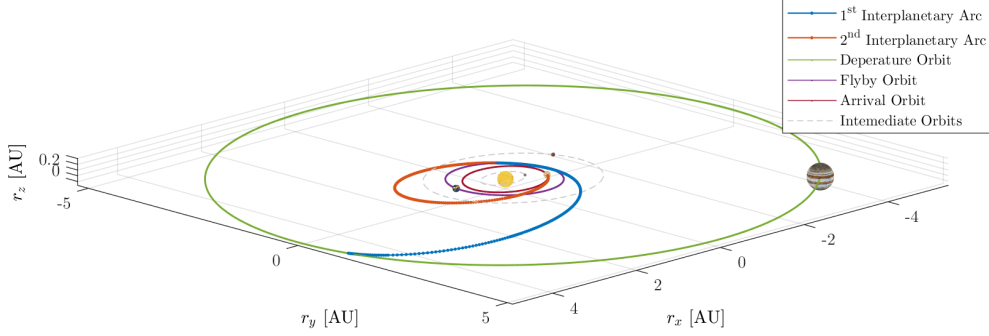


Figure 4: The relative positions of the planets at the date of arrival to Venus with the inclusion of the path taken of the spacecraft during both interplanetary trajectories.

$\Delta V$	Total ToF	$r_p$	Altitude, $h$
0.0012 km/s	1.653854 days	7014.0 km	643.0 km

Table 3: The  $\Delta V$  cost at the perigee, the total time of flight of the PGA manoeuvre, the perigee radius, and altitude above the Earth's surface.

	$a$	$e$	ToF
-	-2428.6 km	3.8881	0.826875 days
+	-2492.2 km	3.8874	0.826979 days

Table 4: The semimajor axis, eccentricity, and time of flight of the incoming and outgoing hyperbolic arms denoted - and +, respectively.

The total time of flight of the PGA manoeuvre was calculated as 1.653854 days and was used to validate the approximation of instantaneous manoeuvre. The total time of flight of the mission is 1401 days therefore, the PGA manoeuvre is only 0.12% of the total time of the mission, justifying the approximation.

### 1.5.2 Total Mission Cost

A collection of all the  $\Delta V$  requirements for the mission is shown in Table 5. It can be seen that the majority of the propellant expenditure is during the departure and arrival of the Jupiter and Venus, respectively. The propellant requirements for the PGA manoeuvre, in comparison to the departure and arrival manoeuvres, is effectively negligible.

	Departure	PGA Manoeuvre	Arrival	Total
$\Delta V$	6.2817 km/s	0.0012 km/s	7.0172 km/s	13.3001 km/s

Table 5: The  $\Delta V$  requirements for the complete mission.

## 1.6 Conclusion

The minima found, although the smallest solution found within the optimisation run, may not be the true global minima within the available domain space. In order to have a true confirmation of a global minima, every combination of departure, flyby, and arrival dates needs to be calculated. Given the large number of combinations the computational time will also be large using the Matlab as the execution platform for the code on a single platform. However, porting the code base to other programming languages such as C++ or Fortran, making use of the parallel computational techniques, and running the ported parallel code on a

computer cluster or multiple servers, can greatly increase the amount of "date space" covered in a similar time frame a single machine running Matlab can do.

As previously stated, these calculations for the minimisation of the  $\Delta V$  were limited due to availability of computational power. But the optimisation algorithm could also be extended to include other variations of the Lambert problem i.e non-zero revolution transfers, which in turn could further reduce the total mission cost.

Furthermore, multiple gravity assists could also be prove useful to additionally reduce the total mission cost. In particular, even making use multiple gravity assists with the departure planet in a similar fashion to the Rosetta mission trajectory, which made use of multiple gravity assists with Earth. This in turn would increase the total time of flight of the mission, but, if this does not represent a concern, could reduce the total mission cost greatly. Moreover, utilising Mars as well as Earth to perform an additional PGA manoeuvre could further reduce the mission cost but adds an additional dimension to compare against increasing the complexity of the model.[3]

In conclusion, the minima obtain via the optimisation algorithm provide a viable solution to transfer from Jupiter to Venus within the constraints set. However, even though this may be the optimum value giving the scope of the model developed, it is not necessarily the best option overall and further refinement in the model to reduce approximations and adding realistic complexity must be conducted.

## 2 Planetary Explorer Mission Analysis

The PoliMi Space Agency has put forward an additional study to conduct an analysis of an orbit around Earth, with perturbations, and the produced ground tracks. The orbit to model has been provided and consists of the keplerian elements shown in Table 6. The ground tracks for this given orbit will be analysed leading to repeating ground tracks. The perturbations to model are the J2 effect produced by the non-spherical mass distribution of the Earth and the drag contribution due to the atmosphere around Earth. The scope of this report will study the effect of the perturbations on the provided orbit in both keplerian parameters and cartesian coordinates to develop a model which will be compared to real satellite orbital data.

$a$	$e$	$i$	$\Omega$	$\omega$	$\theta$	$T_{Period}$	$k : m$	$C_D$	$A/m$
25697 km	0.7242	28.5389°	100°	30°	45°	11.3876 hours	11 : 5	2.2	0.06 [m <sup>2</sup> /kg]

Table 6: The orbital elements to analysis with  $a$ ,  $e$ ,  $i$ ,  $\Omega$ ,  $\omega$ ,  $\theta$ , and  $T_{Period}$  being the standard notations of semimajor axis, eccentricity, inclination, right ascension of ascending node, argument of perigee, true anomaly, and orbital period, respectively. For the analysis of repeating ground tracks the ratio,  $k : m$ ,  $C_D$  and  $A/m$  correspond to the drag coefficient and area to mass ratio, respectively, and are employed within the calculations for drag perturbations.

### 2.1 Ground track analysis

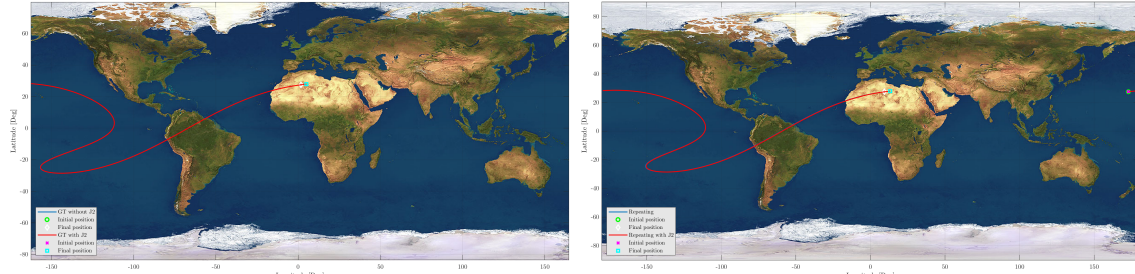
An orbital ground track is the projection of a satellite orbit onto the Earth's surface. At a given instant, the corresponding ground track point is located by its latitude and its longitude relative to the rotating Earth.

#### 2.1.1 Orbital ground tracks with and without the secular J2 effect

In the ideal unperturbed case, the elements defining the orbit remain constant for every revolution. However, due to the rotation of Earth, there are variations between two consecutive orbits when viewing their corresponding ground tracks. The ground tracks appear to deviate westward with an angular displacement,  $\Delta\lambda$ , given by the equation,

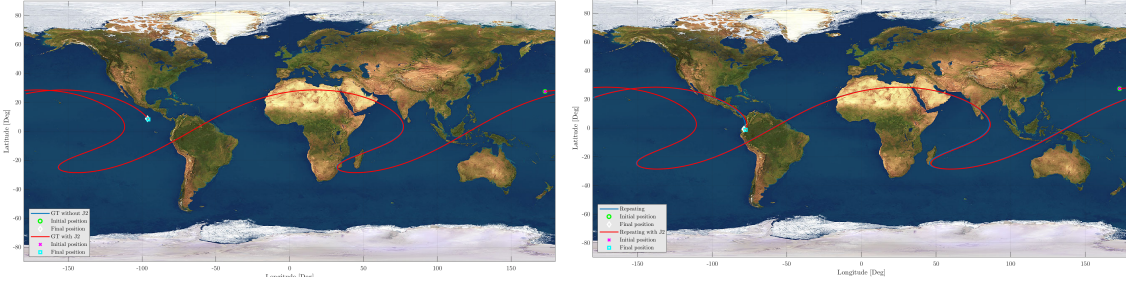
$$\Delta\lambda = T\omega_E \quad (6)$$

where  $T$  is the orbital period of the corresponding orbiting body and  $\omega_E$  is the angular velocity of the Earth. Using the orbital parameters given in Table 6  $\Delta\lambda$  is found to equal 171.2898°.



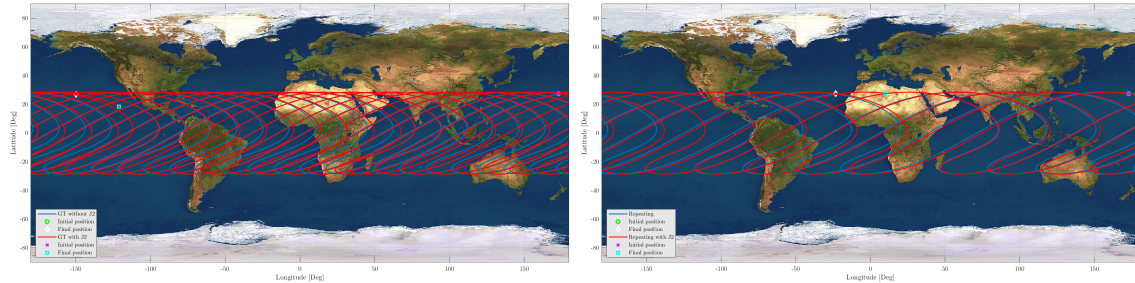
(a) One orbit ground track with and without the J2 effect  
(b) One orbit repeating ground track with and without the J2 effect

Figure 5: One orbit ground tracks



(a) One day ground track with and without the J2 effect (b) One day repeating ground track with and without the J2 effect

Figure 6: One day ground tracks



(a) Ten days ground track with and without the J2 effect (b) Ten days repeating ground track with and without the J2 effect

Figure 7: Ten day ground tracks

The oblateness of the Earth leads to the secular J2 effect which causes variations in the orbital parameters of the right ascension of the ascending node and the argument of perigee. As the orbit of prograde nature, the line of nodes will drift westward while the apse line will advance in the direction of motion.

### 2.1.2 Repeating ground track

For repeating ground tracks, the satellite must complete a number of orbits in a single day equal to the assigned ratio. In order to achieve this, the ratio of the satellite's orbital period must equate the Earth's rotational period. The ratio for this analysis,  $k : m$ , is presented in Table 6.

Therefore, the semi-major axis must be modified in order to achieve the desired value of orbital period. The unaltered ratio for the current orbit is 2.1017, with a semi-major axis of 25697 km, therefore, only minimal adjustments must be made. For a repeating ground track of ratio, 2.2, a semi-major axis of 24926 km was found with a  $\Delta\lambda$  equal to 163.6364°.

### 2.1.3 Repeating ground track with the secular J2 effect

Including the secular J2 effect, an implicit solution for semi-major axis, eccentricity and inclination is

$$\frac{m}{k} = \frac{\omega_E - \dot{\Omega}}{n + \dot{\omega} + \dot{M}} \quad (7)$$

with  $m/k$  equal to the inverse of the repeating ground track ratio,  $\dot{\Omega}, \dot{\omega}, \dot{M}$  are the secular evolution of the right ascension of the ascending node, argument of perigee and mean anomaly and  $n$  is the mean motion.

In particular, eccentricity and inclination are kept constant, while the semi-major axis will be changed. The implicit equation is solved and the calculated value is equal to 24894 km. For the repeating ground track considering the secular J2 effect,  $\Delta\lambda$  is equal to  $163.3270^\circ$ . From the images, it is very evident that the ground tracks are not repeating each other for the reasons said above. The ground track results are shown in Figures 5b, 6b, and 7b.

## 2.2 Integration of the Equations of Motion

The integration can be done using the initial conditions of the satellite in two different frameworks: a Cartesian and a Keplerian. The Cartesian method demonstrates the variance in position and velocity of the orbiting body, whilst the Keplerian focusing on the orbital elements.

### 2.2.1 Cartesian Framework

In this case, the standard two body equations of motion with an additional orbital perturbing accelerations, as shown in Equations 8 and 9, were employed within Matlab and integrated using the *ode113* algorithm provided by Matlab.

$$\ddot{\vec{r}} + \frac{\mu}{r^3} \vec{r} - \sum \vec{a}_p = 0 \quad (8)$$

$$\sum \vec{a}_p = \vec{a}_{drag} + \vec{a}_{J_2} \quad (9)$$

The initial position and velocity were obtained by converting the Keplerian orbital elements to the Cartesian reference frame. The drag perturbations were calculated using the following expression,

$$\vec{a}_{drag} = -\frac{1}{2} \frac{A_{cross} C_D}{m} \rho(h, t) v_{rel}^2 \frac{\vec{v}_{rel}}{v_{rel}} \quad (10)$$

$$\vec{v}_{rel} = \frac{d\vec{r}}{dt} - \vec{\omega}_E \times \vec{r} \quad (11)$$

where  $\omega_e$ , as before, is the Earth rotation velocity around its spin axis. The  $J_2$  components in the Cartesian frame are represented by

$$a_{J2_x} = \frac{3}{2} \frac{J_2 \mu R^2}{r^4} \frac{x}{r} \left( 5 \frac{z^2}{r^2} - 1 \right) \quad (12)$$

$$a_{J2_y} = \frac{3}{2} \frac{J_2 \mu R^2}{r^4} \frac{y}{r} \left( 5 \frac{z^2}{r^2} - 1 \right) \quad (13)$$

$$a_{J2_z} = \frac{3}{2} \frac{J_2 \mu R^2}{r^4} \frac{z}{r} \left( 5 \frac{z^2}{r^2} - 3 \right) \quad (14)$$

In order to fully analyse the propagation of the equations of motion, the results for the Cartesian integration and converted into Keplerian elements.[2]

### 2.2.2 Keplerian Framework

The Keplerian elements represent the physical evolution of the orbit. Considering the fact that the drag is a non-conservative perturbation, the equations that represent the evolution of the Keplerian parameters are the Gauss planetary equations,

$$\frac{dh}{dt} = rp_t \quad (15)$$

$$\frac{de}{dt} = \frac{h}{\mu} \sin(\theta) p_n + \frac{1}{\mu h} [(h^2 + \mu r) \cos(\theta) + \mu e r] p_t \quad (16)$$

$$\frac{di}{dt} = \frac{r}{h} \cos(\omega + \theta) p_h \quad (17)$$

$$\frac{d\Omega}{dt} = \frac{r}{h \sin(i)} \sin(\omega + \theta) p_h \quad (18)$$

$$\frac{d\omega}{dt} = -\frac{1}{eh} \left[ \frac{h^2}{\mu} \cos(\theta) p_n - \left( r + \frac{h^2}{\mu} \right) \sin(\theta) p_t \right] - \frac{r \sin(\omega + \theta)}{h \tan(i)} p_h \quad (19)$$

$$\frac{d\theta}{dt} = \frac{h}{r^2} + \frac{1}{eh} \left[ \frac{h^2}{\mu} \cos(\theta) p_n - \left( r + \frac{h^2}{\mu} \right) \sin(\theta) p_t \right] \quad (20)$$

These equations were integrated over the same time period as those in the Cartesian framework. The perturbation components within the Gauss planetary equations are denoted  $p_t$ ,  $p_n$ , and  $p_h$ . The drag contributions are obtain by calculating the components within the Cartesian frame and translating them to the  $tnh$ -frame.[2] The  $J_2$  perturbations however, are expressed in the appropriate frame and are expressed as,

$$p_n = \frac{\mu}{r^2} \frac{3}{2} J_2 \left( \frac{R_E}{r} \right)^2 [1 - 3 \sin^2(i) \sin^2(\omega + \theta)] \quad (21)$$

$$p_t = -\frac{\mu}{r^2} \frac{3}{2} J_2 \left( \frac{R_E}{r} \right)^2 \sin^2(i) \sin[2(\omega + \theta)] \quad (22)$$

$$p_h = -\frac{\mu}{r^2} \frac{3}{2} J_2 \left( \frac{R_E}{r} \right)^2 \sin(2i) \sin(\omega + \theta) \quad (23)$$

The Keplerian was too integrated with the *ode113* and the comparison between the two reference frames regarding the variation of the orbital elements are shown in Figures 8 - 13.

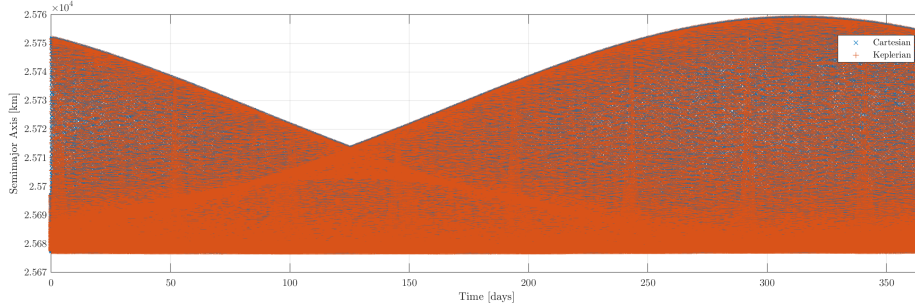


Figure 8: Comparison of the semi-major axis for the Cartesian and Keplerian integrations over one year.

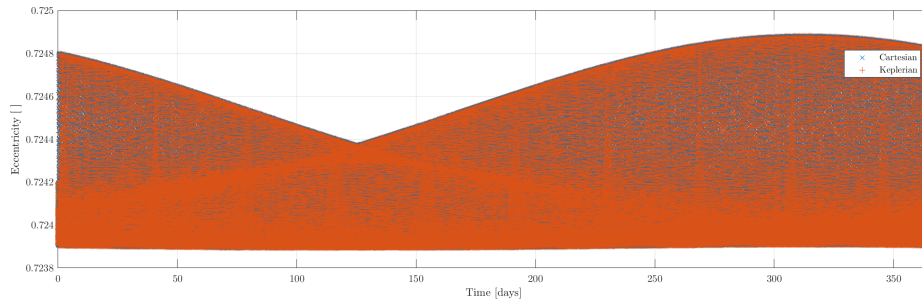


Figure 9: Comparison of the eccentricity for the Cartesian and Keplerian integrations over one year.

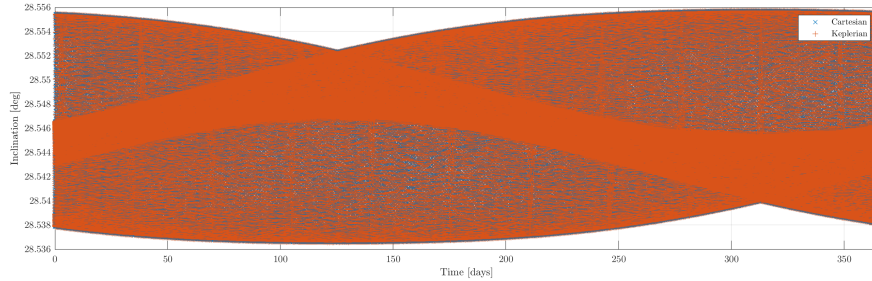


Figure 10: Comparison of the inclination for the Cartesian and Keplerian integrations over one year.

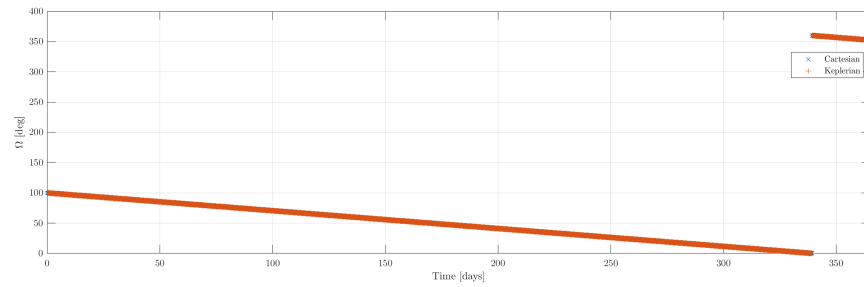


Figure 11: Comparison of the right ascension for the ascending node for the Cartesian and Keplerian integrations over one year.

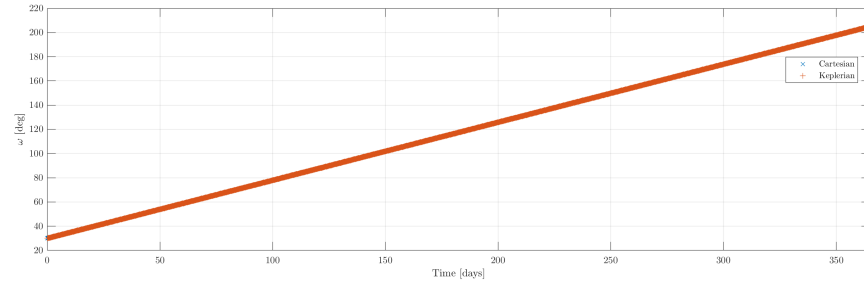


Figure 12: Comparison of the argument of perigee for the Cartesian and Keplerian integrations over one year.

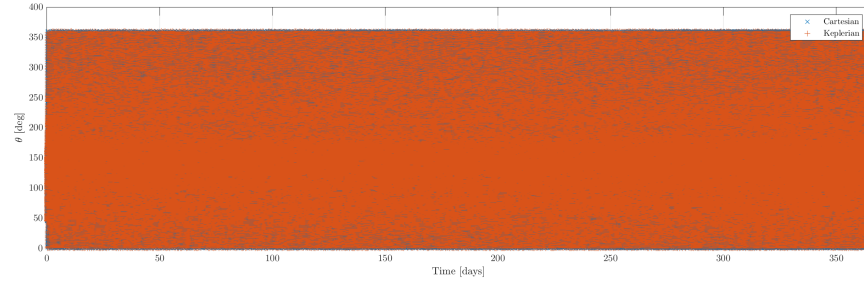


Figure 13: Comparison of the true anomaly for the Cartesian and Keplerian integrations over one year.

## 2.3 Orbit Propagation

The integrations indicate a slight variance in the semi-major axis, eccentricity, and inclination during each orbit producing a sinusoidal, broadband spectrum-like, evolution of the orbital elements. The major evolution within the orbital elements can be seen in right ascension of the ascending node and the argument of perigee with a strong linear trend throughout the integration period. Within an ideal orbit all of the parameters remain constant, with the exception of the true anomaly, therefore any perturbational variances in the true anomaly are more difficult to analyse without more in-depth analysis.

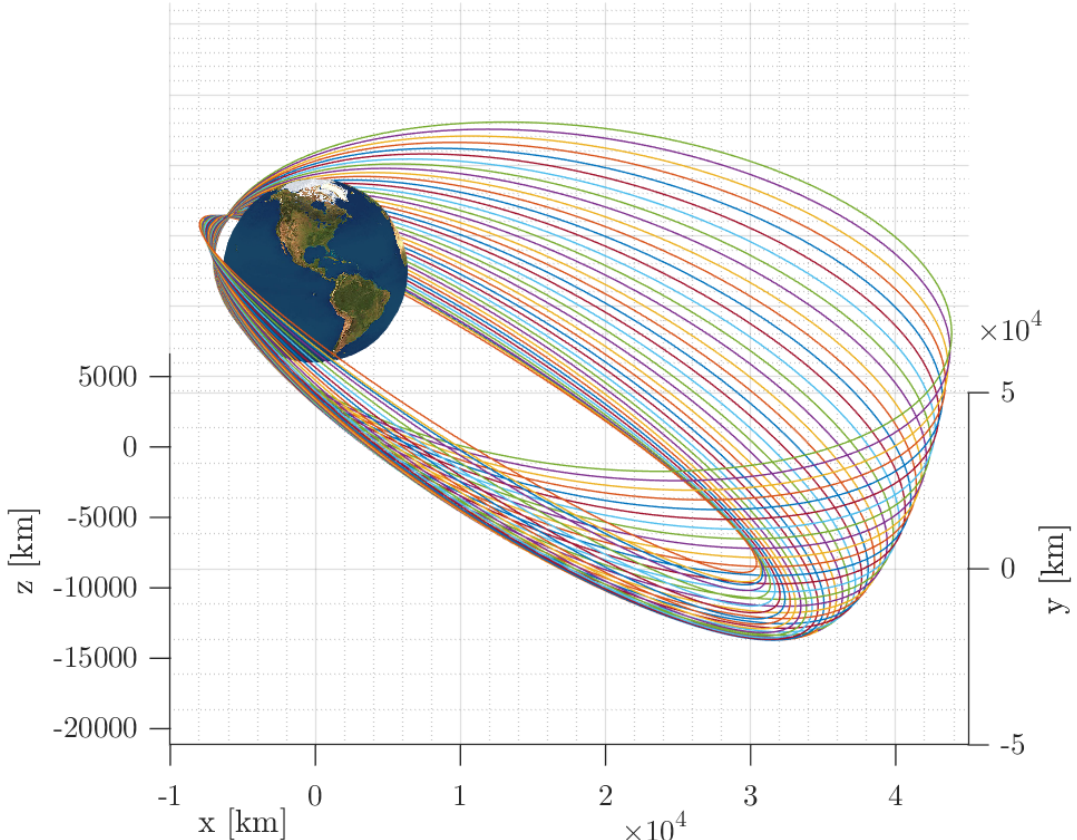


Figure 14: A visual representation of the evolution of a perturbed orbit with snapshots of the orbit over a period of 600 days with 15 day intervals.

## 2.4 Error and Computational Cost Analysis

An analysis of the computational cost between the two integration frameworks was conducted. This was performed by running the integration for varying amount of days, 50 - 2000 days with intervals of days and measuring the time required for completion with the results shown in Figure 15. This analysis was performed on a laptop with i7-8650U processor using Matlab 2019b. The results are reasonably consistent with each other for integrations for up to 900 days with a strong linear trend for the two frameworks.

The relative differences for the between the each integration for the each of the orbital elements for an intergration period of 1000 days were calculated and shown in Table 7. These values were found using the aforementioned *ode113* within Matlab with tolerances  $Tol_{Rel}$  and  $Tol_{abs}$  set to  $10^{-15}$  and  $10^{-16}$ , respectively.

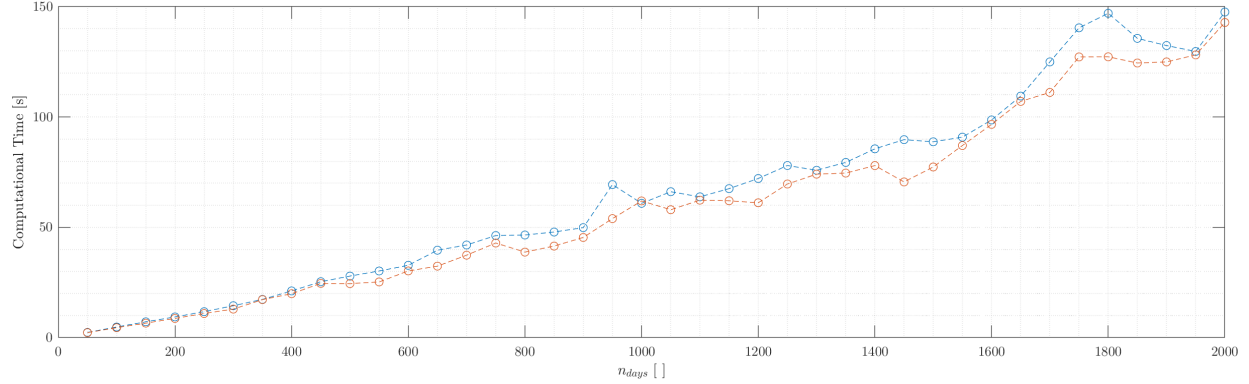


Figure 15: The relative computational costs between the Cartesian, blue, and Keplerian, orange, integrations for varying amounts of integration periods.

	$a$	$e$	$i$	$\Omega$	$\omega$	$\theta$
$\ error_{1000}\ $	0.0079 km	9.5021E-08	7.1946E-07°	5.9051E-07°	6.0396E-06°	0.0064°

Table 7: The relative error between the two integration methods for each of the orbital elements for a period of 1000 days.

## 2.5 Spectral analysis

A complete set of data for both the Cartesian and Keplerian frames were further analysed by the use of a Fast Fourier Transformation (FFT) providing a more clear image of the frequencies involved for a given perturbed orbit. The results of this FFT analysis is shown in the Tables 16 - 21.

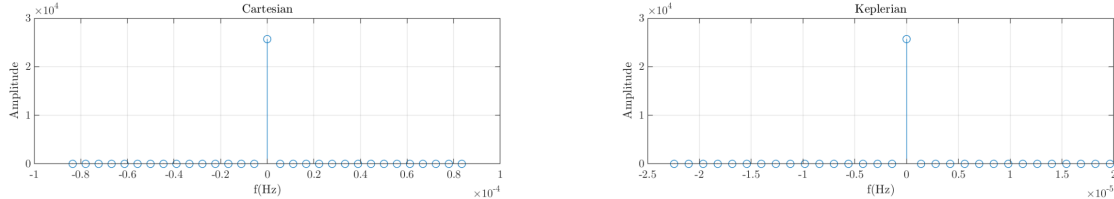


Figure 16: Fourier spectra analyses of the semi-major axis.

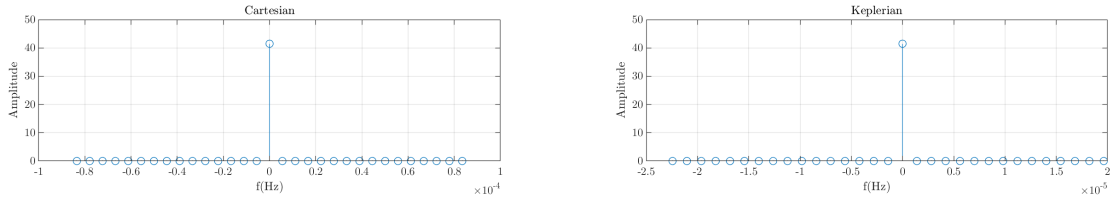


Figure 17: Fourier spectra analyses of the eccentricity.

The figures shown are focused on the central values as the higher frequencies have negligible amplitudes and therefore are less significant over the periods consideration. The frequency domain however, is on the order of magnitude of  $10^5$ . The different scales between the two sets of graphs are due to a disparity in

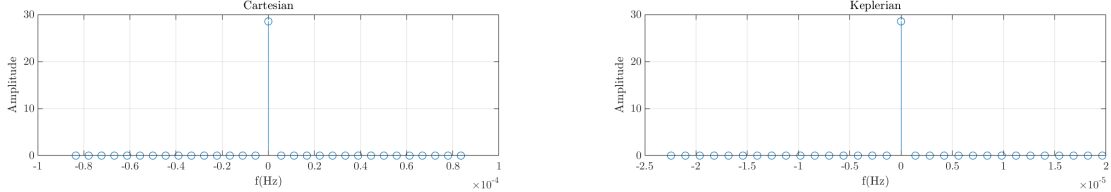


Figure 18: Fourier spectra analyses of the Inclination

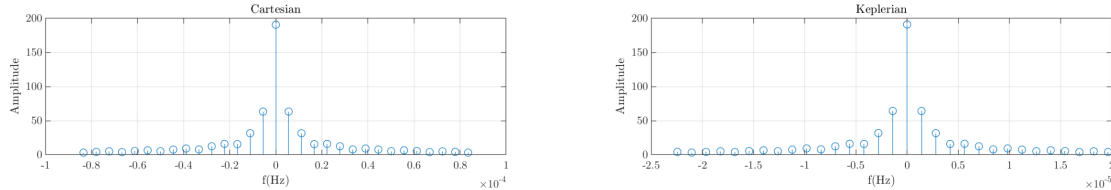


Figure 19: Fourier spectra analyses of the right ascension of the ascending node.

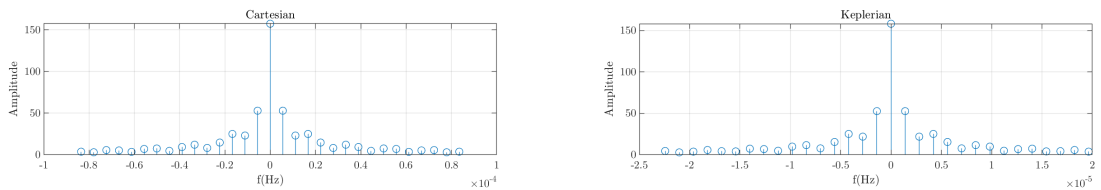


Figure 20: Fourier spectra analyses of the argument of perigee.

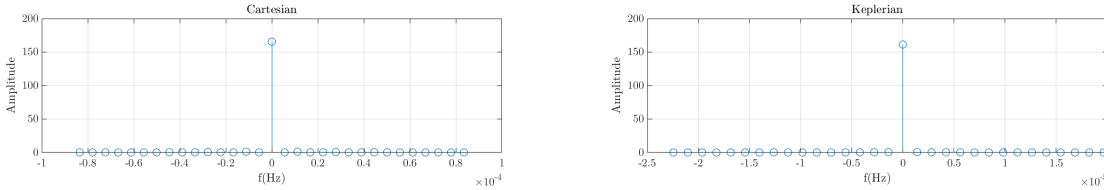


Figure 21: Fourier spectra analyses of the true anomaly.

the sampling frequencies, which occurs on account of the *ode113* algorithm. Although the calculation is performed over the same period, the algorithm produces a discrepancy in the number of data points for the integrations as different sets of equations are integrated.

Referring back and comparing to the Figures 8 - 13 previously shown. The semimajor axis, eccentricity, and inclination variations are small and are of high frequencies thus generating a broadband spectrum-like about a constant value at corresponding to 0 Hz, or in physical sense, the non-perturbing element in question. The right ascension of the ascending node and argument of perigee tell a different story as much lower frequencies with non-negligible amplitudes come into effect due to the perturbations causing the drift.

## 2.6 Filtering of high frequencies

As discussed briefly in the previous section, the orbital elements contain high frequency elements which can be removed by applying a moving average, and remove part of the spectrum and employing an Inverse Fast Fourier Transform (IFFT). The moving average algorithm and IFFT were both applied within the Matlab platform and this process is comparable to low pass filtering. This was performed on the integrations for a period of one year with the results shown in Figure 22. The averaging was performed over orbital period, as

a consequence removing all of the relatively high frequency effects not linked to the long term effects.

$$T = 2\pi \sqrt{\frac{a^3}{\mu_{Earth}}} \quad (24)$$

From this process are obtained the following graph:

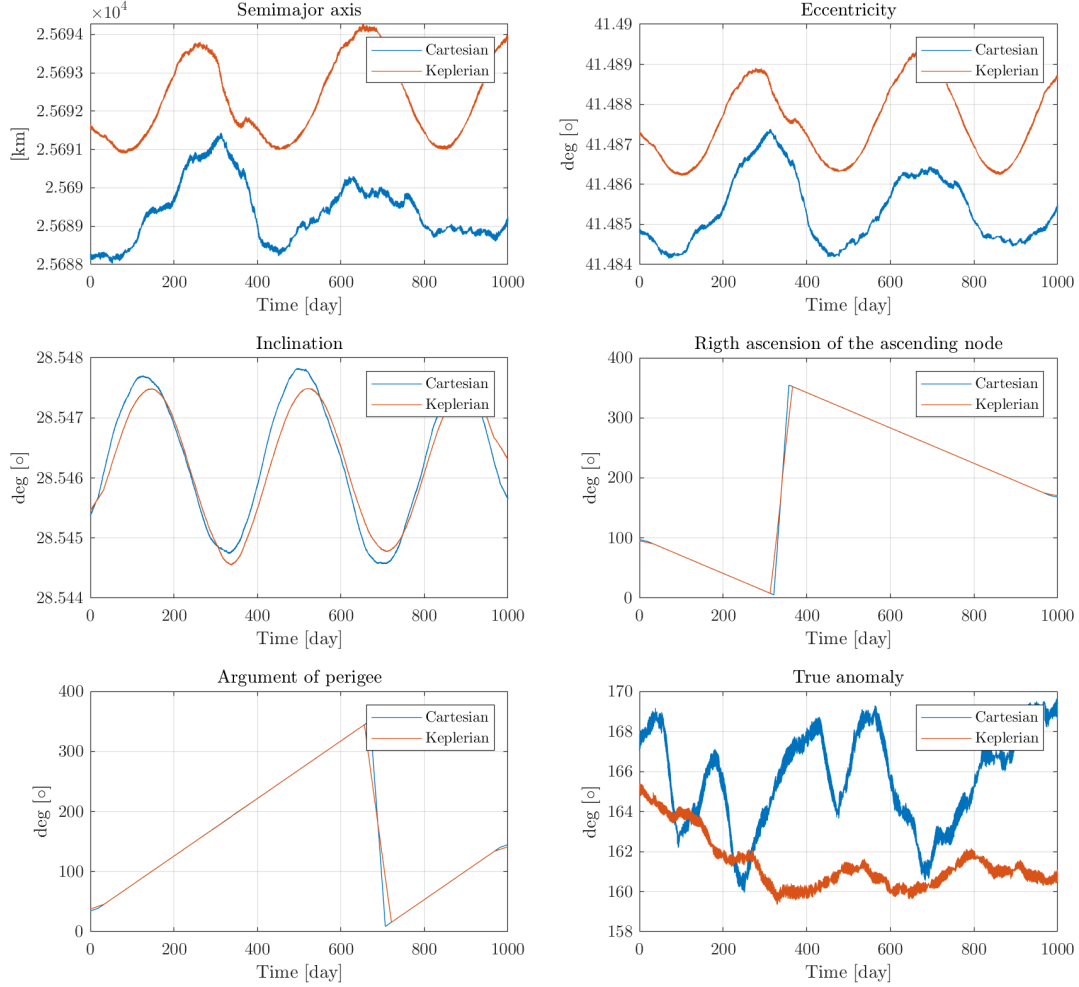


Figure 22: Filtered Cartesian parameters

The main effect of the drag perturbation reduces the energy of the orbit, leading to a natural re-entry trajectory, on account of the non-conservative nature of drag effects. This is a long term effect and will, over time, reduce the energy of the orbit with increasing strength as the satellite achieves a lower orbit. The drag perturbation is a much longer effect in comparison to the  $J_2$  effect which perturbs the orbit every orbital period.

The  $J_2$  perturbation affects only a few of the keplerian elements, not all, therefore, there are special cases in which neither of the elements are affected such as the exploitation of the Molnyia orbit to un-alter the

argument of perigee. Unfortunately, this case in question is not under the class of *Frozen Orbit*, hence the variation of the argument of perigee and right ascension of the ascending node.

In addition, with this further analysis there is more justification to suggest that the frequencies off-centre for argument of perigee and right ascension of the ascending node, with the moving average and spectra removal process are directly linked to the perturbation effects on the orbit.

Once again, the discrepancies in the Figure 22, are due to FFT and IFFT dealing with different amounts of data points produced by the intergration process for the Cartesian and Keplerian frames.

## 2.7 Comparison with Real Data

Any model requires validation with real world data to improve the confidence in the results provided. The Hubble Telescope has been chosen for this validation process. The initial orbital parameters gathered from (Celestrak.com, 2020) from the date of 01/02/2015 were set as the initial conditions for the integration algorithm and were calculated for a period of one year and shown presented in Table 8. The results comparing the real Hubble orbital data and the intergrations are shown in Figures 23 - 28. The drag coefficient is the value usually used and comes from experimental data, while the area to mass ratio is computed from the dimension of the spacecraft being  $13.2m \times 4.2m$ , while the mass is  $11110kg$ . The comparisons shows general agreement with the exception of the semi-major axis. It is important to note that the resolution of the Hubble data is equal to a data point every 12 hours therefore, some general trends may be clear with short terms effects lost due to large intervals in the data.

$a$	$e$	$i$	$\Omega$	$\omega$	$\theta_0$	$C_D$	$A/m$
6927 km	0.000352	$28.4233^\circ$	$331.6646^\circ$	$272.9870^\circ$	$22.8069^\circ$	2.2	$0.005 [m^2/kg]$

Table 8: The initial conditions to be set to be integrated corresponding to 01/02/2015 orbital parameters of the Hubble telescope.

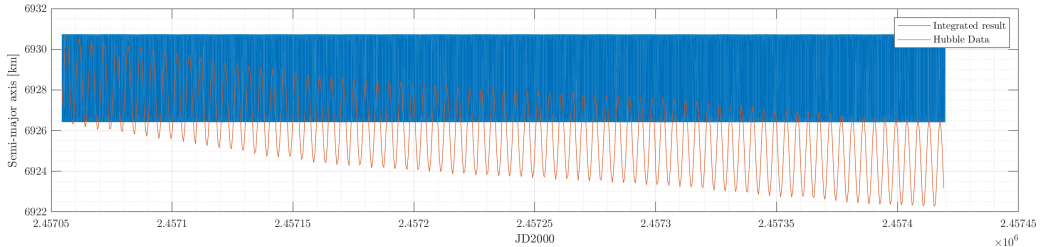


Figure 23: Comparison of the semi-major axis for the Cartesian and Keplerian integrations over one year.

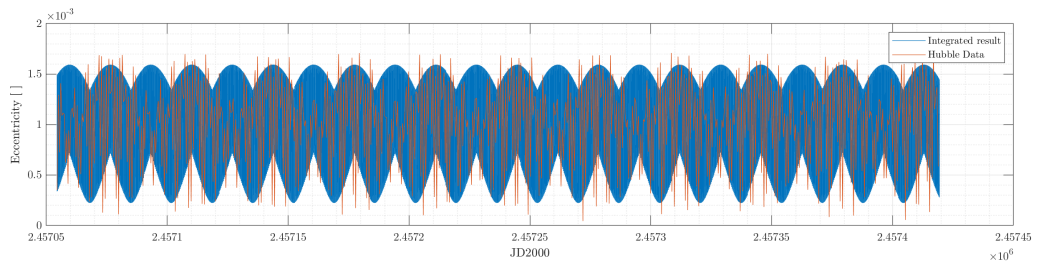


Figure 24: Comparison of the inclination for the Cartesian and Keplerian integrations over one year.

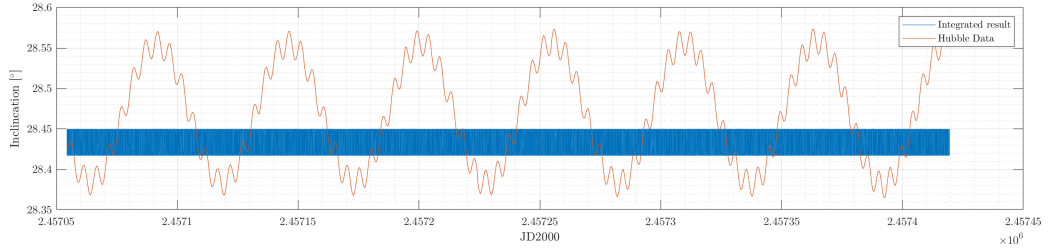


Figure 25: Comparison of the right ascension for the ascending node for the Cartesian and Keplerian integrations over one year.

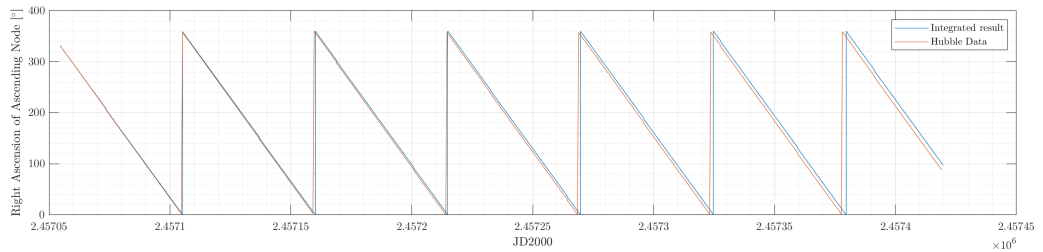


Figure 26: Comparison of the true anomaly for the Cartesian and Keplerian integrations over one year.

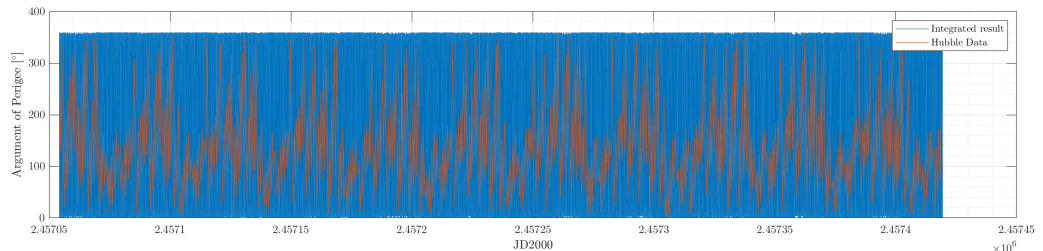


Figure 27: Comparison of the argument of perigee for the Cartesian and Keplerian integrations over one year.

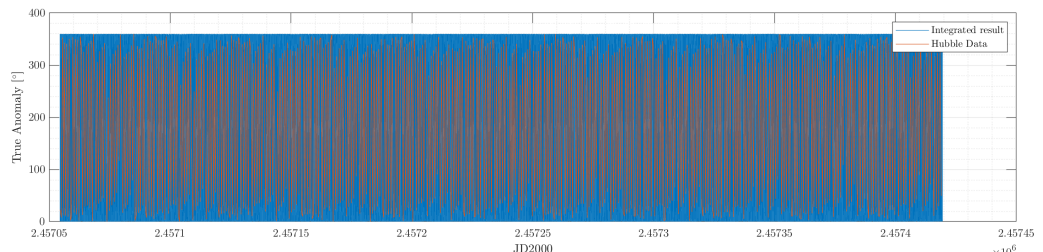


Figure 28: Comparison of the eccentricity for the Cartesian and Keplerian integrations over one year.

In regards of model validation, it is suggested that the model is in good agreement with experimental data for periods of up to one year with larger errors appearing towards the end of the integration period. The right ascension of the ascending node shows some drift towards the end suggesting other factors not implemented are affected the satellite. Similarly with the semi-major axis, the large drift is due to other

perturbation affects yet to be implemented into the model however, the effects over the year are an error of order  $10\text{km}$  so this model can still be used as an estimate of orbital position given the small time spans.

## 2.8 Conclusion

The analyses conducted has shown that the model developed is able to be used for reasonable time periods and still maintain good accuracy using either a Cartesian or Keplerian reference frame. However, even with this there is much future work required in order to improve the model. The perturbations taking into account are only the drag and gravitational  $J_2$  effects. Other affects such as gravitational perturbations due to the moon and solar radiation pressure need also be included to improve the accuracy of this model to the physical world.

The perturbation effects were shown to clearly alter the orbit greatly even over a period of one year, be that is may only, in the argument of perigee and right ascension of the ascending node. The semi-major axis was minimally affected, most likely on account of the position being at such high altitudes that the drag effects had very little affect. Orbits with lower altitudes with the drag perturbation becoming a non-negligible perturbation could be analysed with experimental data of de-orbiting satellites to further validate the model.

Finally, more in depth analysis with much longer integration periods must be conducted in order to quantify the frequencies of the effect of perturbations on an orbit with varying orbital parameters. With this fundamental understanding of the orbital perturbations future orbit and satellite design could make the perturbations an advantage rather than not but, this would greatly depend on the application at hand.

## References

- [1] Hannu Karttunen; et al. (2016). Fundamental Astronomy (6th ed.). Springer. p. 145. Retrieved January 13, 2020.)
- [2] Curtis, H. 2019 Orbital mechanics for engineering students.
- [3] Esa.int. (2020). The long trek. [online] Available at: <https://www.esa.int/> [Accessed 23 Jan. 2020].
- [4] Celestrak.com. (2020). CelesTrak: Current NORAD Two-Line Element Sets. [online] Available at: <https://celestrak.com/NORAD/elements/> [Accessed 28 Jan. 2020].